The Astrophysical Journal Supplement Series, 229:17 (8pp), 2017 March https://doi.org/10.3847/1538-4365/229/1/17

Estimation of the Magnetic Flux Emergence Rate in the Quiet Sun from SUNRISE Data

H. N. Smitha[1], L. S. Anusha[1], S. K. Solanki[1,2], and T. L. Riethmüller[1]
[1] Max-Planck-Institut für Sonnensystemforschung, Justus-von-Liebig-Weg 3, D-37077 Göttingen, Germany; smitha@mps.mpg.de
[2] School of Space Research, Kyung Hee University, Yongin, Gyeonggi, 446-701, Korea
Received 2016 July 19; revised 2016 November 1; accepted 2016 November 19; published 2017 March 22

Abstract

Small-scale internetwork (IN) features are thought to be the major source of fresh magnetic flux in the quiet Sun. During its first science flight in 2009, the balloon-borne observatory SUNRISE captured images of the magnetic fields in the quiet Sun at a high spatial resolution. Using these data we measure the rate at which the IN features bring magnetic flux to the solar surface. In a previous paper it was found that the lowest magnetic flux in small-scale features detected using the SUNRISE observations is 9×10^{14} Mx. This is nearly an order of magnitude smaller than the smallest fluxes of features detected in observations from the *Hinode* satellite. In this paper, we compute the flux emergence rate (FER) by accounting for such small fluxes, which was not possible before SUNRISE. By tracking the features with fluxes in the range 10^{15}–10^{18} Mx, we measure an FER of 1100 Mx cm^{-2} day^{-1}. The smaller features with fluxes $\leqslant 10^{16}$ Mx are found to be the dominant contributors to the solar magnetic flux. The FER found here is an order of magnitude higher than the rate from *Hinode*, obtained with a similar feature tracking technique. A wider comparison with the literature shows, however, that the exact technique of determining the rate of the appearance of new flux can lead to results that differ by up to two orders of magnitude, even when applied to similar data. The causes of this discrepancy are discussed and first qualitative explanations proposed.

Key words: Sun: atmosphere – Sun: magnetic fields – Sun: photosphere

1. Introduction

The quiet Sun covers most of the solar surface, in particular at activity minimum, but also plays an important role even during the active phase of the solar cycle. The magnetic field in the quiet Sun is composed of the network (Sheeley 1967), internetwork (IN, Livingston & Harvey 1971, 1975), and the ephemeral regions (Harvey & Martin 1973). For an overview of the small-scale magnetic features, see Solanki (1993), de Wijn et al. (2009), Priest (2014), and Wiegelmann et al. (2014).

The IN features are observed within the supergranular cells and carry hecto-Gauss fields (Solanki et al. 1996, Khomenko et al. 2003, Martínez González et al. 2008b) although kilo-Gauss fields have also been observed in the IN (Lagg et al. 2010, 2016). They evolve as unipolar and bipolar features with typical lifetimes of less than 10 minutes (Zhou et al. 2010; Lamb et al. 2013; Anusha et al. 2017), i.e., they continuously bring new flux to the solar surface, flux that has been either freshly generated, or recycled. They carry fluxes $\leqslant 10^{18}$ Mx, with the lower limit on the smallest flux decreasing with increasing spatial resolution and polarimetric sensitivity of the observing instruments, although the identification technique also plays an important role.

Ephemeral regions are bipolar magnetic features appearing within the supergranular cells carrying fluxes $\approx 10^{19}$ Mx (Chae et al. 2001; Hagenaar et al. 2003) and are much longer-lived compared to the IN features, with lifetimes of 3–4.4 hr (Title 2000; Hagenaar 2001). The ephemeral regions also bring new magnetic flux to the solar surface.

The network is more stable, with typical lifetimes of its structure of a few hours to a day, although the individual kG magnetic elements within the network live for a much shorter time, as the entire flux within the network is exchanged within a period of 8–24 hr (Hagenaar et al. 2003; Gošić et al. 2014). The flux in the network is fed by ephemeral regions (Schrijver et al. 1997; Hagenaar 2001) and IN features (Gošić et al. 2014). The network features are found along the supergranular boundaries and carry fields of kG strength with a typical flux of 10^{18} Mx (Wang et al. 1995).

The magnetic flux is produced by a dynamo, the location of which is currently the subject of debate, as is whether there is only a single dynamo acting in the Sun (e.g., Stenflo 2012) or whether there is a small-scale dynamo acting in addition to a global dynamo (Petrovay & Szakaly 1993; Cattaneo 1999; Cattaneo & Hughes 2001; Vögler & Schüssler 2007; Schüssler & Vögler 2008; Danilovic et al. 2010; Buehler et al. 2013; Hotta et al. 2015; Karak & Brandenburg 2016). In addition, it is unclear if all the magnetic flux appearing on the Sun is actually new flux produced by a dynamo, or possibly recycled flux transported under the surface to a new location, where it appears again (e.g., Ploner et al. 2001). This may be particularly important at the smallest scales.

An important parameter constraining the production of magnetic flux is the amount of magnetic flux appearing at the solar surface. In particular, the emergence of magnetic flux at very small scales in the quiet Sun provides a probe for a possible small-scale dynamo acting at or not very far below the solar surface. The deep minimum between solar cycles 23 and 24 offered a particularly good chance to study such flux emergence, as the long absence of almost any activity would suggest that most of the emerging flux is newly produced and not transported from decaying active regions to the quiet Sun (although the recycling of some flux from ephemeral regions cannot be ruled out).

The IN quiet Sun displays by far the largest magnetic flux emergence rate (FER). Zirin (1987) pointed out that two orders of magnitude more flux appears in ephemeral regions than in active regions, while the FER in the IN is another two orders of magnitude larger. This result is supported by more recent studies (e.g., Socas-Navarro & Sánchez Almeida 2002; de Wijn

et al. 2009; Parnell et al. 2009; Thornton & Parnell 2011). Given the huge emergence rate of the magnetic flux in the IN, it is of prime importance to measure the amount of flux that is brought to the surface by these features.

The current estimates of the FER in the IN vary over a wide range, which include: 10^{24} Mx day^{-1} (Zirin 1987), 3.7×10^{24} Mx day^{-1} (120 Mx cm^{-2} day^{-1}, Gošić et al. 2016) and 3.8×10^{26} Mx day^{-1} (Zhou et al. 2013). By considering all the magnetic features (small-scale features and active regions), Thornton & Parnell (2011) measure a global FER of 3×10^{25} Mx day^{-1} (450 Mx cm^{-2} day^{-1}), while Thornton (2011) measures 3.9×10^{24} Mx day^{-1} (64 Mx cm^{-2} day^{-1}), whereby almost all of this flux emerged in the form of small IN magnetic features. The FER depends on the observations and the method used to measure it. A detailed comparison of the FERs from different works is presented Section 4.3.

To estimate the FER, Zirin (1987) and Thornton & Parnell (2011) considered features with fluxes $\geqslant 10^{16}$ Mx, while Zhou et al. (2013) and Gošić et al. (2016) included features with fluxes as low as 6×10^{15} Mx and 6.5×10^{15} Mx (M. Gošić 2017, private communication), respectively. However, with the launch of the balloon-borne SUNRISE observatory in 2009 (Solanki et al. 2010; Barthol et al. 2011; Berkefeld et al. 2011; Gandorfer et al. 2011) carrying the Imaging Magnetograph eXperiment (IMaX, Martínez Pillet et al. 2011), it has now become possible to estimate the FER including the contribution of IN features with fluxes as low as 9×10^{14} Mx (Anusha et al. 2017, hereafter referred to as LSA17). The IMaX instrument has provided unprecedented high-resolution magnetograms of the quiet Sun observed at 5250 Å. The high resolution is the main reason for the lower limiting flux. A detailed statistical analysis of the IN features observed in Stokes V recorded by SUNRISE/IMaX is carried out in LSA17. In the present paper we estimate the FER in the IN region using the same data.

In Section 2 we briefly describe the employed SUNRISE data. The IN features bringing flux to the solar surface that are considered in the estimation of FER are outlined in Section 3. The FER from SUNRISE are presented, discussed, and compared with previously obtained results in Section 4 while our conclusions are presented in Section 5.

2. Data

The data used here were obtained during the first science flight of SUNRISE described by Solanki et al. (2010). We consider 42 maps of the line-of-sight (LOS) magnetic field, $B_{\rm LOS}$, obtained from sets of images in the four Stokes parameters recorded with the IMaX instrument between 00:36 and 00:59 UT on 2009 June 9 at the solar disk center, with a cadence of 33 s, a spatial resolution of 0.″15–0.″18 (plate scale is 0.″054 per pixel), and an effective field of view (FOV) of $43'' \times 43''$ after phase diversity reconstruction. The data were reconstructed with a point-spread function determined by in-flight phase diversity measurements to correct for the low-order aberrations of the telescope (defocus, coma, astigmatism, etc., see Martínez Pillet et al. 2011). The instrumental noise of the reconstructed data was 3×10^{-3} in units of continuum intensity. For identification of the features, spectral averaging was done which further reduced the noise to $\sigma = 1.5 \times 10^{-3}$. All features with signals above a 2σ threshold, which corresponds to 12 G, were used (Martínez Pillet et al. 2011).

To measure the flux, we use $B_{\rm LOS}$ determined with the center-of-gravity (COG) method (Rees & Semel 1979; Orozco Suárez et al. 2010; LSA17). The inclination of the IN fields has been under debate, with several studies dedicated to measuring their angular distribution. By analyzing the data from *Hinode*, Orozco Suárez et al. (2007) and Lites et al. (2008) concluded the IN fields to be predominantly horizontal. However, using the same data set, Ishikawa & Tsuneta (2011) found some of the IN fields to be vertical. Jafarzadeh et al. (2014) arrived at similar conclusions (vertical inclination) by analyzing the magnetic bright points observed from the first flight of SUNRISE. Variations in the inclination of the IN fields with heliocentric angle (μ) have been reported by Orozco Suárez & Bellot Rubio (2012) and Borrero & Kobel (2013), Stenflo (2013). Isotropic and quasi-isotropic distribution of the IN field inclinations is favored by Martínez González et al. (2008a), using the Fe I 1.56 μm infrared lines, and by Asensio Ramos (2009) and Asensio Ramos & Martínez González (2014) using *Hinode* data. More recently, Danilovic et al. (2016) found the distribution of IN field inclination to be quasi-isotropic by applying 2D inversions on *Hinode* data and comparing them with 3D magnetohydrodynamic simulations. For a detailed review see Borrero et al. (2015).

In the determination of the FER, we use $B_{\rm LOS}$ for consistency and for easier comparison with earlier studies on the FER. Also, the determination of the exact amount of flux carried in horizontal field features is non-trivial and requires estimates of the vertical thickness of these features and the variation of their field strength with height. In addition, if they are loop-like structures (as is suggested by local-dynamo simulations, e.g., Vögler & Schüssler 2007), then there is the danger of counting the flux multiple times if one or both of their footpoints happen to be resolved by the SUNRISE data. We avoid this by considering only the vertical component of the magnetic field. It is likely that we miss the flux carried by unresolved magnetic loops by concentrating on Stokes V, but this problem is suffered by all previous studies of FER and should decrease as the spatial resolution of the observations is increased. With the SUNRISE I data analyzed here having the highest resolution, we expect them to see more of the flux in the footpoints of the very small-scale loops that appear as horizontal fields in *Hinode* and SUNRISE data (Danilovic et al. 2010).

The small-scale features were identified and tracked using the feature tracking code developed in LSA17. For the sake of completeness we summarize the most relevant results from LSA17 as follows. All the features covering at least 5 pixels were considered with Stokes V being larger than 2σ in each pixel. To determine the flux per feature, the $B_{\rm LOS}$ averaged over the feature, denoted as $\langle B_{\rm LOS} \rangle$ was used. $\langle B_{\rm LOS} \rangle$ had values up to 200 G, even when the maximum field strength in the core of the feature reached kG values. A total of 50,255 features of both polarities were identified. The sizes of the features varied from 5 to 1585 pixels, corresponding to an area range of $\approx 8 \times 10^{-3}$–2.5 Mm^2. The tracked features had lifetimes ranging from 0.55 to 13.2 min. The smallest detected flux of a feature was 9×10^{14} Mx and the largest 2.5×10^{18} Mx.

At the time of the flight of SUNRISE in 2009 the Sun was extremely quiet, with no signs of activity on the solar disk. Two sample magnetograms at 00:47 UT and 00:58 UT are shown in Figure 1. Most of the features in these maps are part of the IN and in this paper, we determine the rate at which they bring flux to the solar surface.

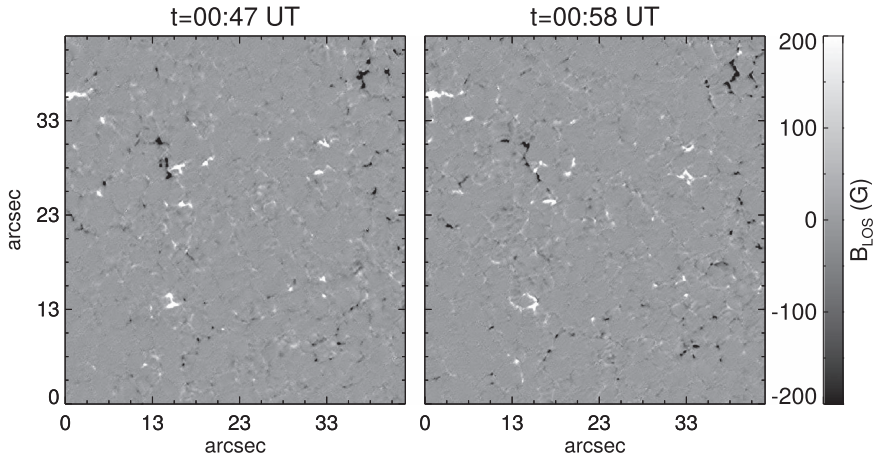

Figure 1. Two sample magnetograms recorded at t = 00:47 UT and 00:58 UT on 2009 June 9 with the SUNRISE/IMaX instrument during its first science flight.

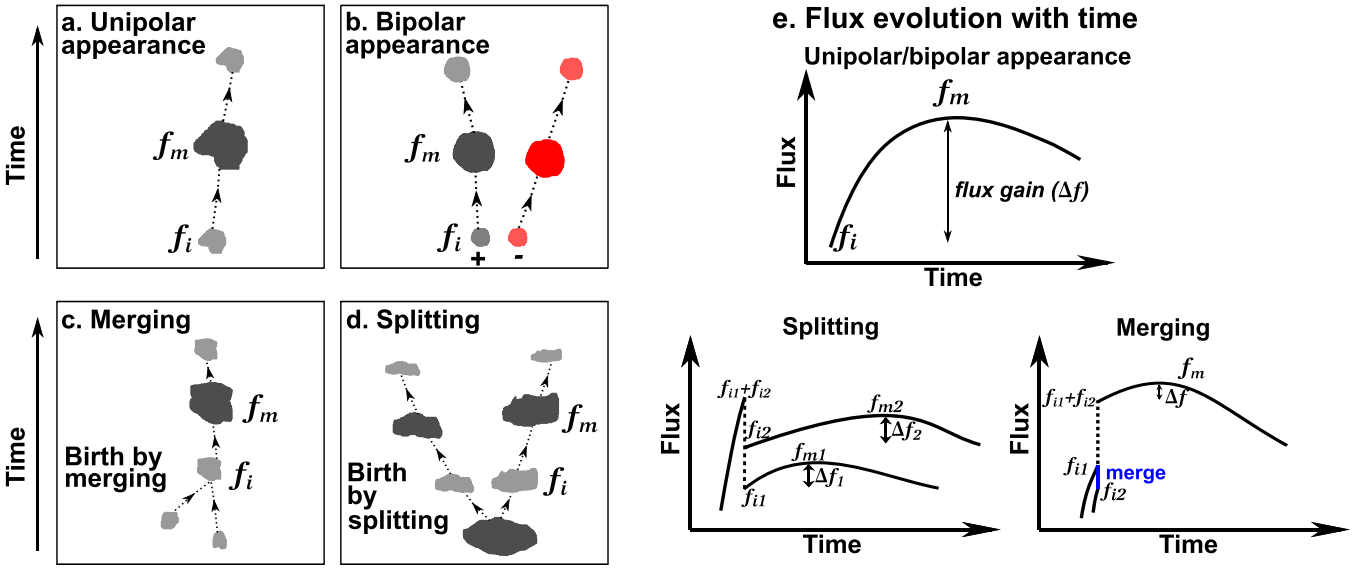

Figure 2. Panels (a)–(d): Schematic representation of the different paths by which magnetic flux is brought to the solar surface and of its subsequent evolution. The quantities f_i and f_m are the instantaneous and maximum fluxes of a feature, respectively, where instantaneous means just after it appears. Panel (e): Typical variation in the flux of a feature, born by unipolar and bipolar appearances (top) and born by splitting/merging (bottom), over time. The flux gained by them after birth is $\Delta f = f_m - f_i$. The features born by splitting carry fluxes $f_{i1,2}$ at birth and reach $f_{m1,2}$ in the course of their lifetime, gaining flux $\Delta f_{1,2}$ after birth. $f_{i1} + f_{i2}$ is equal to the flux of the parent feature at the time of its splitting. The feature born by merging carries flux equal to the sum of the fluxes of the parent features $f_{i1} + f_{i2}$. The blue line indicates the merging of the two features.

3. Processes Increasing Magnetic Flux at the Solar Surface

The different processes increasing the magnetic flux at the solar surface are schematically represented in Figures 2(a)–(d). In the figure, f_i refers to the flux of the feature at its birth and f_m is the maximum flux that a feature attains over its lifetime. A typical evolution of the flux of a feature born by unipolar or bipolar appearances, and by splitting/merging is shown in Figure 2(e) (top and bottom, respectively). The gain in the flux of a feature after its birth is $f_m - f_i$. Magnetic flux at the surface increases through the following processes:

1. Unipolar appearance: birth of an isolated feature with no spatial overlap with any of the existing features in the current and/or previous time frame (Figure 2(a)).
2. Bipolar appearance: birth of bipolar features, with the two polarities closely spaced, and either appearing simultaneously or separated by a couple of time frames (referred to as time symmetric and asymmetric emergence in LSA17; see also Figure 2(b)).
3. Flux gained by features in the course of their lifetime: the gain in the flux of a feature in the course of its lifetime, i.e., the increase in flux between its birth and the time it reaches its maximum flux, before dying in one way or another, either by interacting with another feature, or by disappearing.

   This gain can take place in features born in different ways, be it by growth, or through the merging or splitting of pre-existing features (Figures 2(c)–(e)).

Note that the bipolar appearance of magnetic flux is often referred to as "emergence" in earlier papers including LSA17. However, the term "emergence" in FER describes the appearance of new flux at the solar surface from all three processes described above. To avoid confusion, we refer to the emergence of bipolar features as bipolar appearance. Of all the newly born features over the entire time series, 19,056 features were unique (for area ratio 10:1, see Section 4). Among them 48% (8728 features) were unipolar and 2% (365 features) were part of bipolar

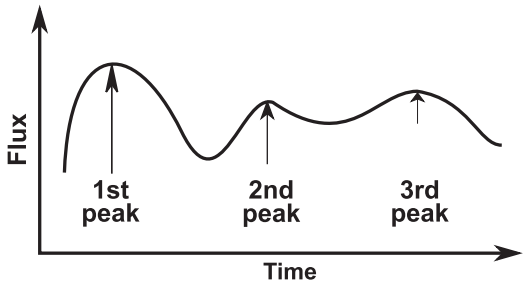

Figure 3. Schematic representation of multiple peaks in the flux of a feature occurring in the course of its lifetime. In the FER estimations, we consider only the largest gain, i.e., flux increase during the first peak in this example.

appearances. Features born by splitting constituted 38% (6718 features), and 12% (2226 features) were born by merging. The remaining 1019 features correspond to those alive in the first frame. A comparison of the rates of birth and death of the features by various processes for different area ratio criteria is given in Table 2 of LSA17.

In the FER estimations, the flux brought by the features born by unipolar and bipolar appearances is the maximum flux that they attain (f_m) over their lifetime. In the case of features born by splitting or merging, the flux gained after birth is taken as the flux brought by them to the surface. This gain is the difference between their flux at birth f_i and the maximum flux they attain f_m, i.e., $f_m - f_i$.

Our approach is conservative in the sense that if a feature reaches multiple peaks of flux in the course of its lifetime, as in the example shown in Figure 3, then we consider only the largest one (the flux gained during the first peak in Figure 3), and neglect increases in flux contributing to smaller peaks such as the second and third peaks in Figure 3. Multiple peaks in the flux of a feature (shown in Figure 3) are rarely seen, as most features do not live long enough to display them (see LSA17).

Changes in the flux of a feature in the course of its lifetime can cause it to seemingly appear and disappear with time if its total flux is close to the threshold set in the study (given by a signal level twice the noise in at least five contiguous pixels). If it disappears and reappears again, then it will be counted twice. This introduces uncertainties in the measurement of the FER. Uncertainties are discussed in Section 4.2.

4. Results and Discussion

4.1. Flux Emergence Rate

In this work, we consider the results from the area ratio criterion 10:1 of LSA17. In that paper, the authors devise area ratio criteria (10:1, 5:1, 3:1 and 2:1) to avoid that a feature dies each and every time that a tiny feature breaks off, or merges with it. For example in a splitting event, the largest of the features formed by splitting must have an area less than n times the area of the second largest, under the n:1 area ratio criterion. We have verified that the choice of the area ratio criterion does not drastically alter the estimated FER, with variations being less than 10% for area ratios varying between 10:1 and 2:1.

The instantaneous and maximum fluxes of the features in different processes are given in Tables 1–5 of LSA17. A summary is repeated in Table 1 for convenience, where fluxes are given for features born by the four processes listed in the first column. The instantaneous flux, in the second column, refers to the flux of a feature at its birth (f_i in Figure 2). In the third column is the maximum flux of a feature during its lifetime (f_m in Figure 2). The flux gain in the fourth column is the difference of the second and third columns ($\Delta f = f_m - f_i$). In the fifth column is the factor by which the flux increases from its birth to its peak (f_m/f_i). The fluxes given in this table are the sum total over all features in the entire time series, for each process.

To compute the FER, we add the fluxes from the various processes described in the previous section. For features born by appearance (unipolar and bipolar), we take their maximum flux (f_m) to be the fresh flux emerging at the surface. For features formed by merging or splitting only the flux increase after birth (Δf) is considered. From the first two processes alone, the total flux brought to the surface is 1.1×10^{20} Mx over an FOV of $43'' \times 43''$ in 22.5 minutes. This gives an FER of 700 Mx cm^{-2} day^{-1}. Including the flux gained by split/merged features increases the FER to 1100 Mx cm^{-2} day^{-1}. Figure 4 shows the contribution from each process to the total FER. The isolated features appearing on the solar surface contribute the largest, nearly 60%. Given that the emerging bipoles contain only 2% of the total observed flux (Table 5 in LSA17), they contribute only about 5.7% to the FER.

However, the flux brought to the solar surface by features born by splitting or merging after their birth is 5×10^{19} Mx, which is quite significant and contributes ≈35% to the FER. The contribution to solar surface flux by this process is comparable to the flux brought to the surface by features born by unipolar appearance (9.7×10^{19} Mx) and nearly an order of magnitude higher than that from features born by bipolar appearance (9.5×10^{18} Mx).

Over their lifetimes, the features born by splitting and by merging gain 1.2 times their initial flux (i.e., $f_m = 1.2 \times f_i$). The fluxes gained by features born by appearance relative to their flux at birth is slightly higher (≈2 times, i.e., $f_m = 2 \times f_i$). This is because the initial magnetic flux of the features born by appearance is quite low. The flux at birth of split or merged features is already quite high because the parent features which undergo splitting or merging are at later stages in their lives (see Figure 2(e)). This is also evident from the fact that the average initial flux per feature of the features born by splitting or merging (2.9×10^{16} Mx and 7.4×10^{16} Mx, respectively) is an order of magnitude higher than the average initial flux per feature of the appeared unipolar or bipolar features (5.4×10^{15} Mx, see Table 2 of LSA17).

The fact that the small-scale magnetic features are the dominant source of fresh flux in the quiet photosphere is discussed in several publications (Socas-Navarro & Sánchez Almeida 2002; de Wijn et al. 2009; Parnell et al. 2009; Thornton & Parnell 2011). Our results extend these earlier findings to lower flux per feature values. As shown in Figure 5, over the range 10^{15}–10^{18} Mx, nearly 65% of the detected features carry a flux $\leqslant 10^{16}$ Mx (left panel). They are also the dominant contributors to the FER (right panel). In this figure, only the features that are born by unipolar and bipolar appearances are considered. Below 2×10^{15} Mx, we see a drop as we approach the sensitivity limit of the instrument.

4.1.1. Flux Loss Rate

Flux is lost from the solar surface by disappearance, cancellation of opposite polarity features, and decrease in the flux of the features in the course of their evolution (i.e., the opposite process to the "flux gain" described earlier in Section 3). As seen from Tables 3 and 4 of LSA17, the

Table 1
Instantaneous and Maximum Fluxes of the Features, Integrated over All Features and T Frames, in Different Processes Measured in LSA17

Process	Instantaneous Flux (f_i in Mx)	Maximum Flux (f_m in Mx)	Flux Gain ($\Delta f = f_m - f_i$ in Mx)	Factor of Increase (f_m/f_i)
Unipolar appearance	4.69×10^{19}	9.69×10^{19}	4.99×10^{19}	2.06
Splitting	1.76×10^{20}	2.12×10^{20}	3.60×10^{19}	1.20
Merging	1.64×10^{20}	1.85×10^{20}	2.20×10^{19}	1.31
Bipolar appearance	3.85×10^{18}	9.53×10^{18}	5.67×10^{18}	2.47

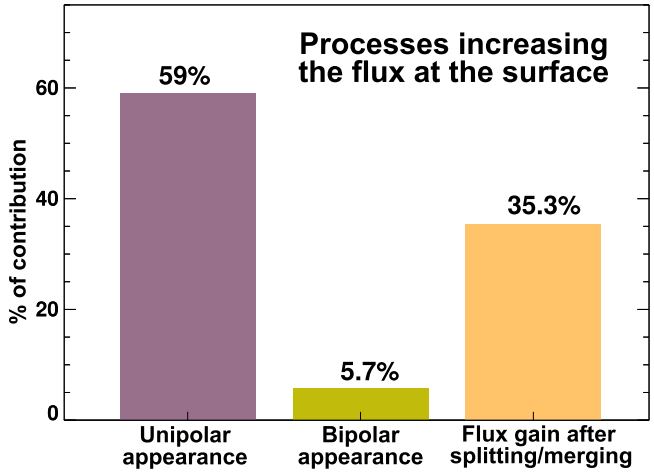

Figure 4. The percentage of contribution to the flux emergence rate (FER) from different processes bringing flux to the solar surface. In the case of unipolar and bipolar appearances, the maximum flux of the feature is used to determine the FER. For the features born by splitting/merging, the flux gained by them after birth is considered. This gain is the difference $f_m - f_i$ in Figures 2(c)–(e).

increase in flux at the solar surface balances the loss of flux, as it obviously must if the total amount of flux is to remain unchanged. To compute the flux loss rate, we take the maximum flux of the features that die by cancellation and by disappearance to be the flux lost by them in the course of their lifetime and during disappearance or cancellation. For the features that die by splitting/merging we take the difference between the maximum flux of the features and the flux at their death as a measure of the flux lost during their lifetimes. By repeating the analyses for the 10:1 area ratio criterion, we find that the flux is lost from the solar surface at a rate of 1150 Mx cm^{-2} day^{-1} which corresponds within 4.5% to the obtained FER. This agreement serves as a consistency check of the FER value that we find.

4.2. Uncertainties

Although most of the uncertainties and ambiguities that arise during feature tracking have been carefully taken care of, as discussed in LSA17, some additional ones which can affect the estimated FER are addressed below.

In our computation of the FER, the features born before the time series began and the features still alive at the end are not considered. According to LSA17, the first and the last frames of the time series had 1019 and 1277 features, respectively. To estimate their contribution, we assume that the features still living at the end have a similar lifetime, size, flux distribution, and formation mechanism as the total number of features studied. We attribute the appropriate average flux at birth and the average flux gain for features born by splitting, merging, unipolar, and bipolar appearance. After including these additional fluxes, we get an FER of ≈1150 Mx cm^{-2} day^{-1}, corresponding to a 4%–5% increase. With this method, we are associating the features with more flux gain than they might actually contribute (as many of them are likely to reach their maximum flux only after the end of the time series). This will be balanced out by not considering the features that are already alive at the beginning (also, it is impossible to determine the birth mechanism of these features).

Furthermore, in the analysis of LSA17, the features touching the spatial boundaries were not counted. An estimate of their contribution, in ways similar to the above, leads to a further increase of the FER by 5%–6%. Thus combining the features in the first and last frames and the features touching spatial boundaries together increase the FER by ≈10%.

Meanwhile, as discussed in Section 3, in the case of flux gained after birth by features born from splitting or merging, we consider only the gain to reach the maximum flux in the feature and not the smaller gains required to reach secondary maximum of flux, if any (see Figure 3). These instances are quite rare. To estimate their contribution, we consider all features living for at least four minutes (eight time steps) so as to distinguish changes in flux from noise fluctuations. They constitute a small fraction of ≈4%. If all these features are assumed to show two maxima of equal strength, then they increase the FER by ≈1.5%. This is a generous estimate and both these assumptions are unlikely to be met. However this is balanced out by not considering the features that have more than two maxima. Thus the increase in FER is quite minor.

Additionally, some of the features identified in a given time frame could disappear, i.e., drop below the noise level, for the next couple of frames, only to reappear after that. This is unlikely to happen due to the thermal or mechanical changes for the SUNRISE observatory, flying in a highly stable environment at float altitude, and with active thermal control of critical elements in the IMaX instrument. As mentioned in Section 3, the appearance and disappearance of features could also occur due to the applied threshold on the signal levels. In our analyses, the reappeared features are treated as newly appeared. This leads to a higher estimation of the FER. Gošić et al. (2016) have estimated that accounting for reappeared features decreases the FER by nearly 10%. If we assume the same amount of decrease in the FER from the reappeared features in our data set, then we finally obtain an FER of 1100 Mx cm^{-2} day^{-1}.

4.3. Comparison with Previous Studies

Below, we compare our results from SUNRISE data with those from the *Hinode* observations analyzed in three recent publications. Although all these papers use observations from the same instrument, they reach very different estimates of FERs. The important distinguishing factor between them is the method that is used to identify the magnetic features and to calculate the FER.

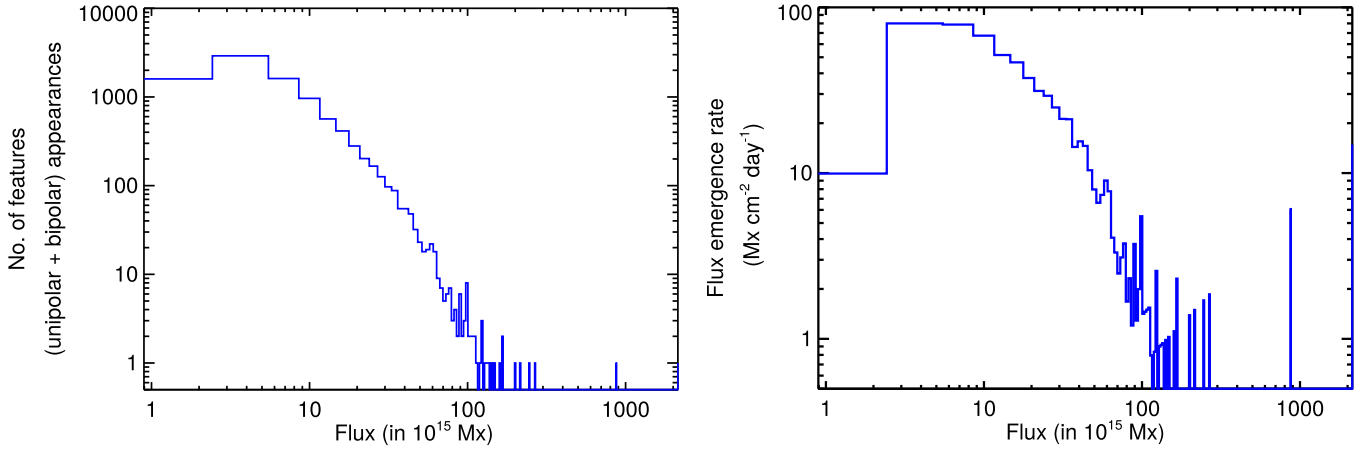

Figure 5. Left panel: histogram of the number of features born by unipolar and bipolar appearances, carrying fluxes in the range 10^{15}–10^{18} Mx. Right panel: the flux emergence rate from the features born by unipolar and bipolar appearances as a function of their flux.

For comparison we summarize the main result that we have obtained here. We find that in the quiet Sun (composed dominantly of the IN) the FER is 1100 Mx cm^{-2} day^{-1}. This corresponds to 6.6 $\times$ 10^{25} Mx day^{-1} under the assumption that the whole Sun is as quiet as the very tranquil SUNRISE/IMaX FOV.

According to Gošić et al. (2016), the flux appearance or emergence rate in the IN region is 120 Mx cm^{-2} day^{-1}, which corresponds to 3.7 $\times$ 10^{24} Mx day^{-1} over the whole surface and the contribution from the IN is assumed to be ≈50%. The authors track individual features and measure their fluxes, which is similar to the method used in LSA17. Their estimate is an order of magnitude lower than the FER obtained in the present paper. This difference can be explained by the higher spatial resolution of SUNRISE compared to *Hinode*. The isolated magnetic feature with the smallest flux detected in SUNRISE/IMaX data is 9 $\times$ 10^{14} Mx (see LSA17), which is nearly an order of magnitude smaller than the limit of 6.5 $\times$ 10^{15} Mx (M. Gošić 2017, private communication), underlying the analysis of Gošić et al. (2016). Additionally, the IMaX data are recorded with 33 s cadence, while the two data sets analyzed by the above authors have cadences of 60 and 90 s each. A higher cadence helps in better tracking of the evolution of features and their fluxes. Also, a significant number of the very short-lived features that we find may have been missed by Gošić et al. (2016).

Thornton & Parnell (2011), also using *Hinode* observations, estimate the FER by fitting a power law to the distribution of frequency of emergence (Mx^{-1} cm^{-2} day^{-1}) over a wide range of fluxes (10^{16}–10^{22} Mx, which covers both, small-scale features as well as active regions). It is shown that a single power law index of −2.7 can fit the entire range. Depending on the different emergence detection methods used and described by these authors, such as Bipole Comparison (BC), Tracked Bipolar (TB) and Tracked Cluster (TC), the authors find a wide range of FERs from 32 to 470 Mx cm^{-2} day^{-1} which correspond to 2.0 to 28.7 $\times$ 10^{24} Mx day^{-1} over the whole solar surface (Table 2 of Thornton & Parnell 2011; Thornton 2011). To match their results from *Hinode* with other studies, the authors choose an FER of 450 Mx cm^{-2} day^{-1}, from the higher end of the range (C. Parnell 2017, private communication). This is nearly four times higher than the value quoted in Gošić et al. (2016), who also used the *Hinode* observations and a smaller minimum flux per feature, so that they should in principle have caught more emerging features. However, Thornton (2011), using a power-law distribution similar to that of Thornton & Parnell (2011) and a slightly different index of −2.5, estimates an FER of 64 Mx cm^{-2} day^{-1}. A possible reason for this difference, as briefly discussed in both these studies, could be the different feature tracking and identification methods used. In Thornton & Parnell (2011), all the features identified by the BC, TB, and TC methods are considered in determining the FER. According to the authors, the BC method counts the same feature multiple times and over-estimates the rate of flux emergence. However in Thornton (2011), only the features tracked by the TB method are used. The large differences in the FERs from the three detection methods quoted in Table 2 of Thornton & Parnell (2011) support this line of reasoning. The FER in Thornton (2011) is roughly half that found by Gošić et al. (2016) and hence is at least in qualitative agreement. The FER estimated by us is 2.5 times higher than the largest value obtained by Thornton & Parnell (2011) and 17 times higher than that of Thornton (2011).

Another recent estimate of the FER is by Zhou et al. (2013). Using *Hinode* observations, they estimate that the IN fields contribute up to 3.8 $\times$ 10^{26} Mx day^{-1} to the solar surface. This is an order of magnitude higher than the global FER of 3 $\times$ 10^{25} Mx day^{-1} published by Thornton & Parnell (2011) and is two orders of magnitude higher than the 3.7 $\times$ 10^{24} Mx day^{-1} obtained by Gošić et al. (2016). In Zhou et al. (2013), it is assumed that every three minutes, the IN features replenish the flux at the solar surface with an average flux density of 12.4 G (Mx cm^{-2}). Here, three minutes is taken as the average lifetime of the IN features (Zhou et al. 2010). Their FER is nearly six times higher than our estimate, although the lowest flux per feature to which *Hinode*/SOT is sensitive is significantly larger than for SUNRISE/IMaX (due to the lower spatial resolution of the former). To understand this difference, we applied the method of Zhou et al. (2013) to the SUNRISE/IMaX observations. From the entire time series, the total sum of the flux in all features with flux >9 $\times$ 10^{14} Mx is 1.1 $\times$ 10^{21} Mx over an area of 3.9 $\times$ 10^{20} cm^2. This gives us an average flux density of 2.8 G, which is 4.5 times smaller than 12.4 G of Zhou et al. (2013). If the IN features are assumed to have an average lifetime of three minutes, similar to Zhou et al. (2013), then FER over the whole solar surface is 8.2 $\times$ 10^{25} Mx day^{-1}. This is 1.2 times higher than our original

estimate from the feature tracking method. If instead, we take the average lifetime of the features in our data set from first appearance to final disappearance at the surface of ≈1.8 minutes, we get an FER of 1.38×10^{26} Mx day^{-1}, nearly 1.9 times higher than our original estimate and still 2.8 times smaller thanthat of Zhou et al. (2013). This is longer than the value of 1.1 minute quoted in LSA17, which includes death of a feature by splitting or merging (see LSA17), i.e., processes that do not remove flux from the solar surface.

To be sure that the problem does not lie in the COG technique employed here, we also estimated the average flux density by considering the $B_{\rm LOS}$ from the recently available inversions of the SUNRISE data (Kahil et al. 2017). The $B_{\rm LOS}$ values returned by the inversions differ from those given by the COG technique by about 5% on average (individual pixels show much larger differences, of course), so that this cannot explain the difference to the value adopted by Zhou et al. (2013). If all the pixels, including noise, are considered then the average flux density is 10.7 G. This is an absolute upper limit of the average flux density as a large part of it is due to noise and it is still lower than the 6IN signal of 12.4 G, estimated by Zhou et al. (2013).

Thus the high value of the FER from Zhou et al. (2013) is at least partly due to their possibly too high value of average flux density. The observations analyzed by these authors clearly show network and enhanced network features. If some of these are misidentified, then this would result in a higher average flux density. If this is indeed the case, then the estimate of the lifetime of three minutes may also be too short (the technique of Zhou et al. 2013 neglects any possible correlation between magnetic flux and lifetime of a feature). Although the amount of flux in IN fields is not expected to change significantly with time or place (see Buehler et al. 2013), this is not true for the amount of flux in the network, which changes significantly. For example, another time series taken by SUNRISE during its first flight, having slightly more network in the FOV, is found to have an average $B_{\rm LOS}$ of around 16 G (including noise), which is higher than the 12.4 G used by Zhou et al. (2013). However, this is just a qualitative assessment and the very large FER found by Zhou et al. (2013) needs to be probed quantitatively in a future study.

5. Conclusions

In this paper, we have estimated the FER in the quiet Sun from the IN features using the observations from SUNRISE/IMaX recorded during its first science flight in 2009. We have included the contribution from features with fluxes in the range 9×10^{14}–2.5×10^{18} Mx, whose evolution was followed directly. By accounting for the three important processes that bring flux to the solar surface: unipolar and bipolar appearances, and flux gained after birth by features born by splitting or merging over their lifetime, we estimate an FER of 1100 Mx cm^{-2} day^{-1}. The third process is found to contribute significantly to the FER. The smaller features with fluxes $\leqslant 10^{16}$ Mx bring most of the flux to the surface. Since our studies include fluxes nearly an order of magnitude smaller than the smallest flux measured from the *Hinode* data, our FER is also an order of magnitude higher when compared to studies using a similar technique (i.e., Gošić et al. 2016). We compare also with other estimates of the FER in the literature. Thornton & Parnell (2011) obtained a range of values. Those near the lower end of the range (also quoted by Thornton 2011), which are possibly the more reliable ones, are roughly consistent with the results of Gošić et al. (2016). The high FER of 3.8×10^{26} Mx day^{-1} found by Zhou et al. (2013) is, however, difficult to reconcile with any other study. It is likely so high partly due to the excessively large $B_{\rm LOS}$ of IN fields of 12.4 G used by these authors, which is more than a factor of 4 times larger than the averaged $B_{\rm LOS}$ of 2.8 G that we find. Even the absolute upper limit of the spatially averaged $B_{\rm LOS}$ in our data (including noise) is below the value used by Zhou et al. (2013). We therefore expect that they have overestimated the FER.

There is clearly a need for further investigation, not only to better quantify the reasons for the different results obtained by different techniques. There are also still multiple open questions. What is the cause of the increase and decrease of the flux of a feature during its lifetime? Is this due to interaction with "hidden" flux? Is this hidden flux not visible because it is weak and thus below the noise threshold, or because it is structured at very small scales, i.e., it is below the spatial resolution? How strongly does the "hidden" or missed flux change with changing spatial resolution? The most promising approach to answering these and related questions is to study the flux evolution in a magnetohydrodynamic simulation that includes a working small-scale turbulent dynamo.

We thank F. Kahil for helping with the comparison of COG and inversion results. H.N.S. and L.S.A. acknowledge the financial support from the Alexander von Humboldt foundation. The German contribution to SUNRISE and its reflight was funded by the Max Planck Foundation, the Strategic Innovations Fund of the President of the Max Planck Society (MPG), DLR, and private donations by supporting members of the Max Planck Society, which is gratefully acknowledged. The Spanish contribution was funded by the Ministerio de Economía y Competitividad under Projects ESP2013-47349-C6 and ESP2014-56169-C6, partially using European FEDER funds. The HAO contribution was partly funded through NASA grant number NNX13AE95G. This work was partly supported by the BK21 plus program through the National Research Foundation (NRF) funded by the Ministry of Education of Korea.

References

Anusha, L. S., Solanki, S. K., Hirzberger, J., & Feller, A. 2017, A&A, 598, A47
Asensio Ramos, A. 2009, ApJ, 701, 1032
Asensio Ramos, A., & Martínez González, M. J. 2014, A&A, 572, A98
Barthol, P., Gandorfer, A., Solanki, S. K., et al. 2011, SoPh, 268, 1
Berkefeld, T., Schmidt, W., Soltau, D., et al. 2011, SoPh, 268, 103
Borrero, J. M., Jafarzadeh, S., Schüssler, M., & Solanki, S. K. 2015, SSRv, 113
Borrero, J. M., & Kobel, P. 2013, A&A, 550, A98
Buehler, D., Lagg, A., & Solanki, S. K. 2013, A&A, 555, A33
Cattaneo, F. 1999, ApJL, 515, L39
Cattaneo, F., & Hughes, D. W. 2001, A&G, 42, 18
Chae, J., Martin, S. F., Yun, H. S., et al. 2001, ApJ, 548, 497
Danilovic, S., Schüssler, M., & Solanki, S. K. 2010, A&A, 513, A1
Danilovic, S., van Noort, M., & Rempel, M. 2016, A&A, 593, A93
de Wijn, A. G., Stenflo, J. O., Solanki, S. K., & Tsuneta, S. 2009, SSRv, 144, 275
Gandorfer, A., Grauf, B., Barthol, P., et al. 2011, SoPh, 268, 35
Gošić, M., Bellot Rubio, L. R., del Toro Iniesta, J. C., Orozco Suárez, D., & Katsukawa, Y. 2016, ApJ, 820, 35
Gošić, M., Bellot Rubio, L. R., Orozco Suárez, D., Katsukawa, Y., & del Toro Iniesta, J. C. 2014, ApJ, 797, 49
Hagenaar, H. J. 2001, ApJ, 555, 448
Hagenaar, H. J., Schrijver, C. J., & Title, A. M. 2003, ApJ, 584, 1107
Harvey, K. L., & Martin, S. F. 1973, SoPh, 32, 389
Hotta, H., Rempel, M., & Yokoyama, T. 2015, ApJ, 803, 42

Ishikawa, R., & Tsuneta, S. 2011, ApJ, 735, 74
Jafarzadeh, S., Solanki, S. K., Lagg, A., et al. 2014, A&A, 569, A105
Kahil, F., Riethmüller, T. L., & Solanki, S. K. 2017, ApJS, 229, 12
Karak, B. B., & Brandenburg, A. 2016, ApJ, 816, 28
Khomenko, E. V., Collados, M., Solanki, S. K., Lagg, A., & Trujillo Bueno, J. 2003, A&A, 408, 1115
Lagg, A., Solanki, S. K., Doerr, H. P., et al. 2016, A&A, 596, 13
Lagg, A., Solanki, S. K., Riethmüller, T. L., et al. 2010, ApJL, 723, L164
Lamb, D. A., Howard, T. A., DeForest, C. E., Parnell, C. E., & Welsch, B. T. 2013, ApJ, 774, 127
Lites, B. W., Kubo, M., Socas-Navarro, H., et al. 2008, ApJ, 672, 1237
Livingston, W., & Harvey, J. 1971, in IAU Symp. 43, Solar Magnetic Fields, ed. R. Howard (Dordrecht: Reidel), 51
Livingston, W. C., & Harvey, J. 1975, BAAS, 7, 346
Martínez González, M. J., Asensio Ramos, A., López Ariste, A., & Manso Sainz, R. 2008a, A&A, 479, 229
Martínez González, M. J., Collados, M., Ruiz Cobo, B., & Beck, C. 2008b, A&A, 477, 953
Martínez Pillet, V., Del Toro Iniesta, J. C., Álvarez-Herrero, A., et al. 2011, SoPh, 268, 57
Orozco Suárez, D., & Bellot Rubio, L. R. 2012, ApJ, 751, 2
Orozco Suárez, D., Bellot Rubio, L. R., del Toro Iniesta, J. C., et al. 2007, ApJL, 670, L61
Orozco Suárez, D., Bellot Rubio, L. R., Vögler, A., & Del Toro Iniesta, J. C. 2010, A&A, 518, A2
Parnell, C. E., DeForest, C. E., Hagenaar, H. J., et al. 2009, ApJ, 698, 75
Petrovay, K., & Szakaly, G. 1993, A&A, 274, 543
Ploner, S. R. O., Schüssler, M., Solanki, S. K., & Gadun, A. S. 2001, in ASP Conf. Ser. 236, Advanced Solar Polarimetry—Theory, Observation, and Instrumentation, ed. M. Sigwarth (San Francisco, CA: ASP), 363
Priest, E. 2014, Magnetohydrodynamics of the Sun (Cambridge: Cambridge Univ. Press)
Rees, D. E., & Semel, M. D. 1979, A&A, 74, 1
Schrijver, C. J., Title, A. M., van Ballegooijen, A. A., Hagenaar, H. J., & Shine, R. A. 1997, ApJ, 487, 424
Schüssler, M., & Vögler, A. 2008, A&A, 481, L5
Sheeley, N. R., Jr. 1967, SoPh, 1, 171
Socas-Navarro, H., & Sánchez Almeida, J. 2002, ApJ, 565, 1323
Solanki, S. K. 1993, SSRv, 63, 1
Solanki, S. K., Barthol, P., Danilovic, S., et al. 2010, ApJL, 723, L127
Solanki, S. K., Zufferey, D., Lin, H., Rueedi, I., & Kuhn, J. R. 1996, A&A, 310, L33
Stenflo, J. O. 2012, A&A, 547, A93
Stenflo, J. O. 2013, A&A, 555, A132
Thornton, L. M. 2011, PhD thesis, Univ. St. Andrews
Thornton, L. M., & Parnell, C. E. 2011, SoPh, 269, 13
Title, A. 2000, RSPTA, 358, 657
Vögler, A., & Schüssler, M. 2007, A&A, 465, L43
Wang, J., Wang, H., Tang, F., Lee, J. W., & Zirin, H. 1995, SoPh, 160, 277
Wiegelmann, T., Thalmann, J. K., & Solanki, S. K. 2014, A&ARv, 22, 78
Zhou, G., Wang, J., & Jin, C. 2013, SoPh, 283, 273
Zhou, G. P., Wang, J. X., & Jin, C. L. 2010, SoPh, 267, 63
Zirin, H. 1987, SoPh, 110, 101